Uncovering the relationship between the change in heat capacity for enzyme catalysis and vibrational frequency through isotope effect studies

Hannah BL Jones[†Δ], Rory M Crean[#†Δ], Christopher Matthews[†], Anna B Troya[†], Michael J Danson[†], Steven D Bull[‡], Vickery L Arcus[§*], Marc W Van der Kamp[%*] and Christopher R Pudney[†*]

†Department of Biology and Biochemistry, ‡Department of Chemistry, # Doctoral Training Centre in Sustainable Chemical Technologies, University of Bath, Bath BA2 7AY, United Kingdom

§School of Science, Faculty of Science and Engineering, University of Waikato, Hamilton 3240, New Zealand

% School of Biochemistry, University of Bristol, Biomedical Sciences building, University Walk, Bristol BS8 1TD, United Kingdom

ABSTRACT: Understanding how enzyme catalysis varies with temperature is key to understanding catalysis itself, and ultimately, how to tune temperature optima. Temperature dependence studies inform on the change in heat capacity during the reaction, $\Delta C_P^{\ddagger}$, and we have recently demonstrated that this can expose links between the protein free energy landscape and enzyme turnover. By quantifying $\Delta C_P^{\ddagger}$, we capture information on the changes to the distribution of vibrational frequencies during enzyme turnover. The primary experimental tool to probe the role of vibrational modes in a chemical/biological process is isotope effect measurements, since isotopic substitution primarily affects the frequency of vibrational modes at/local to the position of isotopic substitution. We have monitored the temperature dependence of a range of isotope effects on the turnover of a hyper-thermophilic glucose dehydrogenase. We find a progressive effect on the magnitude of $\Delta C_P^{\ddagger}$ with increasing isotopic substitution of D-glucose. Our experimental findings, combined with molecular dynamics simulations and quantum mechanical calculations, demonstrate that $\Delta C_P^{\ddagger}$ is sensitive to isotopic substitution. The magnitude of the change in $\Delta C_P^{\ddagger}$ due to substrate isotopic substitution indicates that small changes in substrate vibrational modes are 'translated' into relatively large changes in the (distribution and/or magnitude of) enzyme vibrational modes along the reaction. Therefore, the data suggest that relatively small substrate isotopic changes are causing a significant change in the temperature dependence of enzymatic rates.

KEYWORDS Heat capacity, isotope effect, enzyme, catalysis, temperature dependence

Isotope effects are one of the most powerful tools to investigate chemical mechanism and the physical chemical underpinnings of catalysis.[1] Enzyme mechanistic studies often employ kinetic and binding isotope effects, KIE and BIE, to access information on specific steps in enzyme catalysis and to test the role of protein 'dynamics' in enzyme turnover.[2–4] The power of isotope effects lies in the simplicity of their physical origin. That is, isotopic substitution decreases the frequency of all vibrational modes, but does not affect the electronic structure of the molecule.[5] Therefore, where one observes an isotope effect, the physical chemical interpretation of the experimental observation is much less ambiguous compared to mutagenesis studies, for example.

In enzymatic studies, the temperature dependence of the KIE is often used to infer the presence or absence of protein motions that affect the rate of enzymatic turnover.[6,7] The microscopic interpretation of these studies is controversial (see e.g. ref. [8]), but at least at a basic level these studies seem to validate the notion that protein motions can affect enzyme turnover (if not necessarily the catalytic step itself). Recently, the potential role of protein 'dynamical' effects on the reaction catalyzed by dihydrofolate reductase (DHFR) or HIV-1 protease, have been assessed based on simulations with mass modulated (isotopically substituted) enzymes.[9–11] In both systems, a small contribution from these dynamical effects to reducing the free energy profile around the transition state of the order ~2 kJ mol^{-1} was found. These authors interpret this difference as arising from the coupling between the reaction coordinate and the degrees of freedom of the system. However, the major contributor to reducing the free energy barrier arises from electrostatic effects.[2,12–14] In addition, Åqvist used simulation to reveal the molecular origin of entropic effects in catalysis with respect to temperature, and illustrated the importance of considering not just the immediate active site, but also remote parts of the protein (and surrounding solvent).[15] We further point out that others have argued that fast (sub-picosecond), local active site protein modes play a role in transition state formation (and thereby catalysis).[16] A further alternative view is that so-called protein dynamical effects are coupled to the reaction coordinate, but provide a small contribution to barrier reduction relative to, e.g., the electrostatic contribution via preorganisation.[2,12–14] Although not a catalytic 'dynamical effect', when strictly defined,[17] differences in enzyme fluctuations (or vibrations) that cause a change in heat capacity along the reaction can affect the temperature dependence of enzyme activity.[18] Understanding this effect in detail may provide new tools to manipulate enzyme optimal temperatures.

We have recently demonstrated how capturing information on the change in heat capacity for activation $\Delta C_P^{\ddagger}$, informs on differences in the distribution of frequencies of vibrational modes between the enzyme-substrate and enzyme-transi-

tion state complex.[19,20] Typically, the temperature dependence of enzyme rate constants is fitted to the Eyring equation.

$$k = (k_B T/h) e^{\Delta S^{\ddagger}/R} e^{-\Delta H^{\ddagger}/RT} \quad \text{Eq 1}$$

This model assumes that $\Delta H^{\ddagger}$ and $\Delta S^{\ddagger}$ are temperature independent. However, if $\Delta H^{\ddagger}$ and $\Delta S^{\ddagger}$ are temperature dependent, then this implies a non-zero value for $\Delta C_P^{\ddagger}$. $\Delta C_P^{\ddagger}$ can be extracted from temperature dependence studies of enzymes fitted using a model that incorporates temperature dependence of $\Delta H^{\ddagger}$ and $\Delta S^{\ddagger}$, which we have termed macromolecular rate theory (MMRT): [21,22]

$$lnk = ln\frac{k_B T}{h} - \left[\frac{\Delta H^{\ddagger}_{T_0} + \Delta C_P^{\ddagger}(T - T_0)}{RT}\right] + \left[\frac{\Delta S^{\ddagger}_{T_0} + \Delta C_P^{\ddagger}(lnT - lnT_0)}{R}\right] \quad \text{Eq 2}$$

where T_0 is an arbitrary reference temperature. $\Delta C_P^{\ddagger}$ is the difference in heat capacity between the ground and transition states. $\Delta C_P^{\ddagger}$ determines the change in $\Delta H^{\ddagger}$ and $\Delta S^{\ddagger}$ with temperature and thereby defines the non-linearity of the temperature dependence of the Gibbs free energy difference between the ground state and the transition state ($\Delta G^{\ddagger}$). Indeed, Roy *et al.* point to a temperature dependent activation entropy as the source of non-linear temperature-dependence plots.[8] Other models that move beyond Eq 1 have been proposed, primarily relating to equilibria of different functional/non-functional states.[23,24] Whilst we do not discount these models, it appears, based on the range of recently published work from different labs,[18–20,22] that Eq 2 is useful and broadly accurate.

We expect that the dominant contribution to $\Delta C_P^{\ddagger}$ in enzymes is the difference in distribution and frequency[21,22] of the large number of vibrational modes of the molecule and its closely associated solvent molecules in the ground and transition states. Alternatively, a negative value of $\Delta C_P^{\ddagger}$ implies that $<(\delta H)^2>$ (the mean squared distribution of enthalpies) for the enzyme substrate complex is greater than $<(\delta H)^2>$ for the enzyme-transition state complex at a given temperature.[22] We suggest that the magnitude of $\Delta C_P^{\ddagger}$ can therefore be used as a proxy for the changes in vibrational modes (distribution, frequency) during enzyme turnover.

The origin of isotope effects lies in the difference in the frequency of vibrational modes between isotope changes. Observing a relationship between (i) increasing isotopic substitution of the substrate, (ii) an isotope effect on the rate of turnover, and (iii) $\Delta C_P^{\ddagger}$ would suggest that the enzymatic $\Delta C_P^{\ddagger}$ is sensitive to (substrate) vibrational modes that affect the observed reaction rate. Bigeleisen considered the effect of isotopic substitution on heat capacity, though not for hydrogen.[25] More recently, Tjahjono and Garland[26] have directly measured the difference in apparent molar heat capacity, C_P^0, for a series of model compounds with different levels of deuterium substitution. As with other reports,[27] the authors find that the deuterium isotope effect on C_P^0 was always positive, i.e. C_P^0 increases with increasing isotopic substitution (Nd) and that the relationship was essentially linear: ΔC_P^0 (J mol^{-1} K^{-1}) = 2.75Nd – 1.52. The increase in C_P^0 is attributed to the increased mass of the isotopologue and the concomitant decrease in frequencies of the affected bonds.

In a recent appraisal of a range of previously published experimental enzyme systems,[20] we found that there was potentially an isotope effect on $\Delta C_P^{\ddagger}$. Longbotham *et al*[28] recently performed a study exploring a range of isotope effects on labelling the flavin in a model flavoenzyme and found their data could only be adequately fitted using Eq 2. These authors find a small isotope effect on $\Delta C_P^{\ddagger}$ outside experimental error for some, but not all, labelling patterns. Based on these intriguing findings we are inspired to explore the potential for isotope effects combined with Eq 2 to inform on changes in enzyme vibrational modes along the chemical reaction coordinate and their relationship to temperature dependence. Herein, we use a hyperthermophilic enzyme, *Sulfolobus solfataricus* glucose dehydrogenase (*ss*GDH) as a model system to explore the contribution of enzymatic isotope effects on heat capacity differences during the reaction. Our data provide an experimental link between the temperature dependence of enzyme turnover and (low frequency) vibrational modes. Importantly, the results raise the question of how subtle localized changes (through isotopic substitutions in the substrate) can lead to a significant change in the enzymatic heat capacity (and thus $<(\delta H)^2>$) during the reaction.

RESULTS AND DISCUSSION

*Hydride transfer in ssGDH is rate determining. ss*GDH is a promiscuous hyperthermophilic enzyme that reduces nicotinamide adenine dinucleotide (phosphate) (NAD(P)$^+$), with a variety of sugars.[29] Milburn *et al*[30] solved the X-ray crystal structure with both NADP$^+$ and glucose/xylose bound using a catalytically inactive variant (T41A). Notionally the reduction of the nicotinamide (C4) occurs as a hydride transfer from C1 of the sugar, concomitant with a proton transfer from the C1 hydroxyl (Scheme S1) to a water molecule or hydroxide ion coordinated by a Zn^{2+} ion. We have performed molecular dynamics simulations of *ss*GDH (Figure 1A) in complex with both glucose and xylose (four independent runs of 50 ns, with all four active sites occupied). From our MD simulations, consistent with the X-ray crystal structures, we find that the hydride donor-acceptor (D-A) distance is very similar for glucose and xylose, but not identical, with the xylose D-A being ~0.2 Å longer (Figure 1B; Supporting information). Specifically, the averages are 2.77 +/- 0.287 Å and 2.93 +/- 0.310 Å; medians are 2.725 Å and 2.895 Å.

Quantum chemical cluster calculations (Figure 1C – 1G) on a 148 atom model of the active site of *ss*GDH in complex with glucose (Figure 1C) suggest a stepwise chemical mechanism, whereby proton abstraction from a Zn^{2+} coordinated hydroxide forms a stable alkoxide intermediate on the

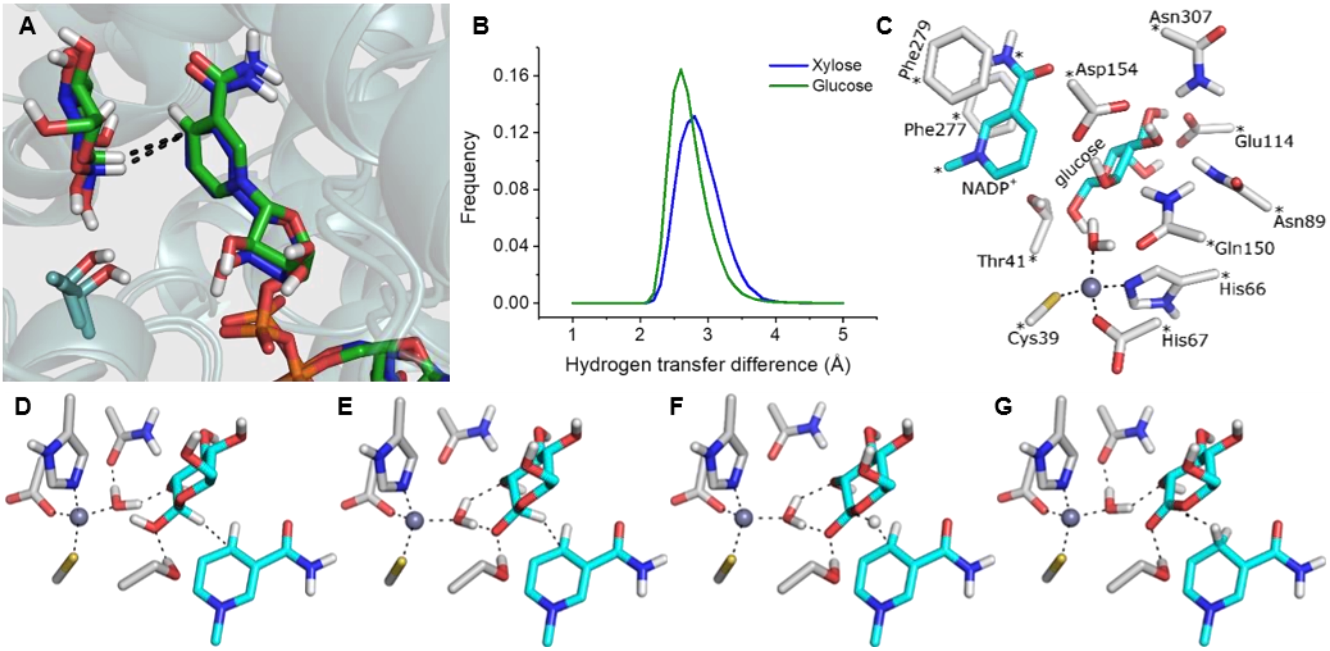

Figure 1. A, Representative structures of glucose (green) and xylose (blue) from our MD simulations demonstrating they have the same binding interface with NADP+. **B,** Normalized histograms (bin width 0.1 Å) of the hydrogen transfer distance of glucose and xylose from MD simulations of *ss*GDH. **C,** QM cluster model created of glucose in complex with NADP+, with asterisks indicating atoms fixed throughout the optimisation process. **D – G,** Reaction mechanism obtained from the QM model, starting from the reactant (**D**), to the deprotonated reactive intermediate (**E**), the transition state (**F**), and finally the product (**G**).

sugar C1 prior to hydride transfer. When a water molecule is modelled as coordinated to the Zn^{2+} ion (Figure 1C), the D-A distance is 2.49 Å, consistent with our MD simulations (above, Figure 1B). When instead a hydroxide ion is modelled as coordinated to the Zn^{2+} ion, the proton on the sugar C1 hydroxyl is readily abstracted upon geometry optimization (Figure 1D) to form a reactive intermediate, with the resulting anion stabilised by hydrogen bonding interactions to the now Zn^{2+} bound water and T41. This reactive intermediate has a reduced D-A distance of 2.22 Å, which reduces further as the glucose and NADP+ rings pucker to form a transition state (Figure 1F) with a predicted free energy barrier relative to the reactive intermediate of 32.6 kJ mol^{-1} at 298 K. In synchrony with the hydride transfer, the Zn^{2+} bound water rotates away from glucose, returning to its original position of hydrogen bonding with Q150 and the C2 hydroxyl of glucono-D-lactone. In order to compare the predicted and experimental activation energies, one must consider the initial deprotonation into the bulk milieu (Reactant to Reactive Intermediate; Figure 1D and E, respectively), which cannot be determined reliably with the cluster based approach due to the importance of inhomogeneous long range interactions in modulating pK_a values.[31] Instead, one can subtract the hydride transfer barrier from the experimental barrier to obtain a predicted pK_a of 7.2 (Full calculation details can be found in the Supporting Information), which is in good agreement with the experimental pH optimum of 8.[32] Finally, we note that there is no obvious role for water in the rate determining step (deprotonated water acts as a base for proton abstraction, whereas the subsequent hydride transfer is rate limiting, see below) and so at least this route is not giving rise to a primary solvent isotope effect (see below).

Our combined computational and kinetic data (discussed below) provide evidence for the mechanistic step observed from our kinetic data. The slightly larger D-A distance in the Michaelis complex for xylose *versus* glucose, calculated from MD simulations, correlates with a ~1.6-fold larger k_{cat} value (k_{cat} = 95 and 58 s^{-1} at 90 °C; Figure 2) and a ~5-fold larger K_m (K_m = 2.5 ±0.3 and 0.5 ± 0.2 mM at 85 °C; Figure S1A and S1B) for glucose *versus* xylose, , respectively. This magnitude increase in rate seems reasonable for a hydride transfer given a ~0.2 Å difference in D-A distance[33,34] (Figure 1B) and implies that the observed rate is primarily capturing the hydride transfer step. Similarly, the difference in K_m is likely reflective of the difference in binding geometry and bonding (discussed below). Our QM cluster calculations provide a reasonable mechanism in which a Zn^{2+} coordinated hydroxide ion can deprotonate the glucose C1 hydroxyl to form a reactive intermediate. The direct nature of the enzyme assay (NADP+ reduction to NADPH), our QM calculations and the observation of a significant primary kinetic isotope effect (KIE, see below) suggests that the kinetic data primarily reflect the hydride transfer step.

Heat capacity changes during enzyme reaction. We have measured the temperature dependence of k_{cat} for both glucose and xylose, fitted to Eq 2, shown in Figure 2A and 2B. For both glucose and xylose, the temperature vs. ln(k_{cat})

data are clearly curved and are therefore appropriately fitted to Eq 2 instead of Eq 1. *ss*GDH is extremely thermally stable[32] and we do not find evidence for unfolding on the

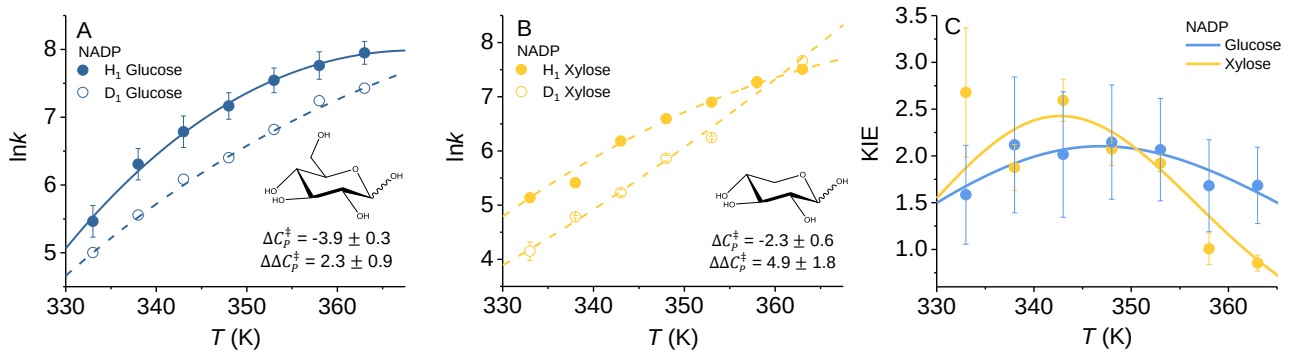

Figure 2. The temperature dependence of NADP+ reduction by glucose (A) and xylose (B). Solid and dashed lines show the fitted to Eq 2 for the protiated and deuterated Glucose/xylose (D^1), respectively. C, the resulting KIE extracted from the lnk_{cat} (ln min^{-1}) in panels A and B. The solid line is the modelled KIE based on the parameters extracted from Eq 2 (Solid lines in panels A and B)

timescales of our assays at any temperature. To capture the curvature in temperature dependence plots accurately, and to capture the experimental system at its natural operating temperature (77 °C)[32], we have focused on the temperature range 60-90 °C. From Figure 2A and 2B we find a significant difference in the magnitude of $\Delta C_P^{\ddagger}$ with $\Delta C_P^{\ddagger}$ = −3.9 ± 0.3 and −2.3 ± 0.6 kJ mol^{-1} K^{-1}, for glucose and xylose, respectively.

Potentially, the difference in $\Delta C_P^{\ddagger}$ between glucose and xylose could arise through a difference in the chemical structure of the sugars, i.e. the additional CH_2OH group of glucose. For example, the hydroxyl of the hydroxymethyl group can form hydrogen bonding interactions with either E114 or H297. This additional interaction may cause a general rigidification of the glucose and the active site, and thus decrease the absolute heat capacity of the ground and transition state. We cannot, however, confidently project how this would change $\Delta C_P^{\ddagger}$ (i.e. how the heat capacity of the ground state is affected differently from the heat capacity of the transition state), and thus cannot assign the physical origin of the observed differences in $\Delta C_P^{\ddagger}$ between glucose and xylose.

Change in $\Delta C_P^{\ddagger}$ with substrate isotopic substitutions. To explore the relation between $\Delta C_P^{\ddagger}$ and substrate vibrational states, we determine the effects of substrate isotope substitutions on $\Delta C_P^{\ddagger}$ of sugar dehydrogenation by *ss*GDH. Figure 2A and 2B show the temperature dependence of the primary kinetic isotope effect (1° KIE) for hydride transfer for both glucose and xylose using D-glucose (D^1) and D-xylose (D^1), respectively. For both sugars, the KIE is temperature-dependent (Figure 2C) and similar in magnitude (~2 – 2.5). Despite the similar magnitude of the KIE for both sugars, the isotope effect (IE) on the magnitude of $\Delta C_P^{\ddagger}$ is significantly different. The 1° IE on $\Delta C_P^{\ddagger}$ is very large for xylose [D-Xylose (D^1)], bringing the $\Delta C_P^{\ddagger}$ value to ~0 within error ($\Delta\Delta C_P^{\ddagger}$ = 4.9 ± 1.8 kJ mol^{-1} K^{-1}). However, for glucose the 1° IE is smaller: D-glucose (D_1) $\Delta C_P^{\ddagger}$ = −1.6 ± 0.6 kJ mol^{-1} K^{-1} ($\Delta\Delta C_P^{\ddagger}$ = 2.3 ± 0.9 kJ mol^{-1} K^{-1}). We note that this trend in the data is recapitulated when omitting 'outlier' data points (Figure S2). Moreover, these data do not appear to be due to significant differences in the structure or bonding of the reactive complex, since the K_m values (Figure S2) are the same within error for the protiated and deuterated substrate, K_m = 3.2 ± 0.4 and 0.7 ± 0.1 mM at 85 °C *c.f.* K_m = 2.5 ±0.3 and 0.5 ± 0.2 mM at 85 °C for glucose *versus* xylose, respectively. The magnitude of $\Delta\Delta C_P^{\ddagger}$ for both xylose and glucose is surprising, as these differences are much larger than can be expected from effects on (substrate) heat-capacity for isotopic substitutions alone (discussed below). It indicates some (unknown) interaction between the reacting species and the enzyme enthalpy distribution that can be perturbed by isotopic substitution.

As discussed previously, the difference in $\Delta C_P^{\ddagger}$ between glucose and xylose could arise through a difference in the

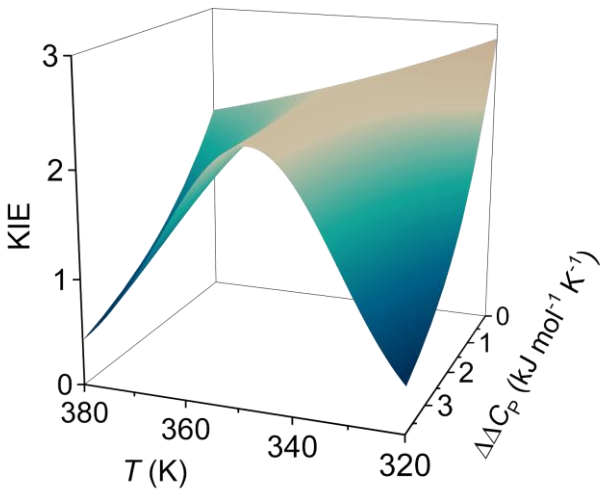

sugar-enzyme interactions. However, isotope effects arise from differences in the frequency of vibrational modes,[5] and not from changes in electronic structure that can lead to additional interactions. At a phenomenological level, our data therefore provide evidence that $\Delta C_P^{\ddagger}$ can be significantly perturbed by the frequency of bond vibrations in the reacting species. Figure 2C shows the KIE as a curve resulting from the temperature dependence parameters extracted from the fits in Figures 2A and 2B.

Figure 3. Numerical model showing how the magnitude of the glucose 1° KIE versus temperature is affected by differences in the isotope effect on $\Delta C_P^{\ddagger}$. $\Delta H^{\ddagger}$ and $\Delta S^{\ddagger}$ values used for modelling given in Table 1.

.

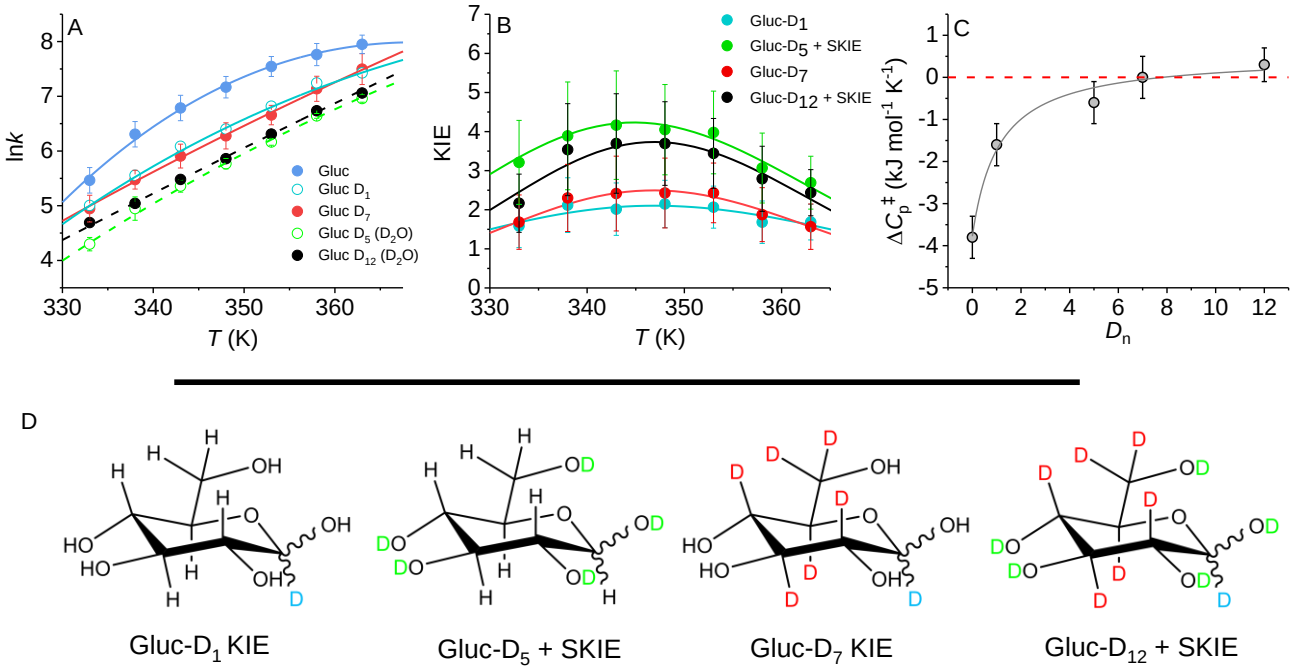

Figure 4. The effect of isotopic labelling on $\Delta\Delta C_P^{\ddagger}$. **A,** The temperature dependence of k_{cat} for each isotopolgue of glucose. Solid lines are fits to Eq 1. **B,** Resulting KIEs extracted from the fits in panel A. **C,** correlation between the increase in molecular mass (through isotopic substitution) and the extracted magnitude of $\Delta\Delta C_P^{\ddagger}$. The solid line is a simple rectangular hyperbola and is to aid the eye only to illustrate the trend. **D**, structures of each isotopolgue used in the panel A.

The temperature dependence of the KIE for both glucose and xylose show a qualitatively similar relationship; curvature with a maximum at 346 and 343 K, respectively. Typically, one observes a decrease in the magnitude of the KIE with respect to temperature when fitting data using the Eying/Arrhenius equation (as shown in Figure S3). Figure 3 shows a numerical model of the data shown in Figure 2C (using Eq 2), where the magnitude of $\Delta C_P^{\ddagger}$ for the isotopolgue is varied to explore a range of $\Delta\Delta C_P^{\ddagger}$ values and the resulting effect on the KIE. From this model, we find that the curvature in the KIE plots is a direct result of the isotope effect on $\Delta C_P^{\ddagger}$. That is, as $\Delta\Delta C_P^{\ddagger}$ tends towards zero (no isotope effect on $\Delta C_P^{\ddagger}$), the KIE plot will become 'normal', showing a decrease in magnitude with increasing temperature (Figure 3). These data show that a consequence of *any* significant isotope effect on $\Delta C_P^{\ddagger}$ is that the KIE will tend towards unity and this is also true for all temperature dependent KIEs fitted using e.g. Eq 1. The difference when accounting for plot curvature is that the KIE will approach unity at both low and high temperatures. It is therefore not surprising that both sugars show a KIE that tends towards 1 at low and high temperatures and this will be the case for all isotope effects on $\Delta C_P^{\ddagger}$.

Effect of increasing isotopic substitution on $\Delta C_P^{\ddagger}$. To explore the relationship between substrate vibrational modes and $\Delta C_P^{\ddagger}$ further, we use glucose to find if there is an isotopic mass dependence on the magnitude of $\Delta C_P^{\ddagger}$. We have increased the isotopic substitution of glucose using both per-deuterated glucose and in combination with deuterium oxide (D_2O) and monitored the temperature dependence of k_{cat} as shown in Figure 4A. The temperature dependence of the KIE is shown in Figure 4B with the corresponding labeled structures shown in Figure 4D. Given that the *ss*GDH mechanism involves a concomitant hydride and proton transfer (discussed above and Figure 1C-G), we have essentially two possible 1° KIEs for the hydride (1^{o}_{H}) and proton

(1^{o}_{P}) transfer. However, we note that our combined experimental and computational evidence above suggests that the proton transfer is fast relative to the hydride transfer, indicating that there would be no primary KIE for proton transfer and the experimental assay thus essentially captures the hydride transfer step.

Labelling of sites distal to the transferred hydride are a secondary (2°) KIE. In the present case, this 2° KIE will be com

Table 1. Kinetic parameters extracted from fits of Eq 1 and 2 to the temperature dependence data shown in Figure 4A

	$\Delta H^{\ddagger}$ (kJ mol^{-1}) [a]	$\Delta S^{\ddagger}$ (kJ mol^{-1} K^{-1}) [a]	$\Delta C_P^{\ddagger}$ (kJ mol^{-1} K^{-1})	KIE [a]	KIE$_{calc}$ [a,d]	$\Delta\Delta H^{\ddagger}$ (kJ mol^{-1} K^{-1})[b] - MMRT	$\Delta\Delta H^{\ddagger}$ (kJ mol^{-1} K^{-1})[c] - Eyring
D-glucose	76.0 ± 2.3	1.33 ± 0.01	-3.8 ± 0.5	–	–	–	–
D_1	78.0 ± 2.1	1.33 ± 0.01	-1.6 ± 0.5	2.1 ± 0.6	2.8	2.0 ± 4.4	1.6 ± 11.7
D_5	86.1 ± 2.5	1.35 ± 0.01	-0.6 ± 0.5	4.0 ± 1.2	0.9	10.1 ± 4.8	7.2 ± 10.6
D_7	80.4 ± 2.0	1.34 ± 0.01	0.0 ± 0.5	2.4 ± 0.9	2.7	4.4 ± 4.4	3.8 ± 9.5
D_{12}	80.4 ± 1.5	1.33 ± 0.01	0.3 ± 0.4	3.7 ± 1.1	2.3	4.4 ± 4.4	0.9 ± 9.5

[a], Data at 348 K. [b], from fits to Eq 2 (MMRT) at 348 K. [c], From fits to Eq 1 (Eyring equation). [d], Calculated from the QM cluster model.

posed of many microscopic 2° KIEs for each labelled position (shown in green in Figure 4D). Finally, to label the exchangeable OH groups we have performed our experiments in D_2O and this will lead to deuteration of *all* exchangeable protons (including amino acid side chains) that are immediately solvent accessible. Note that the enzyme itself is not incubated in D_2O, only the substrate and so the enzyme deuteration occurs only on the timescale of the steady-state assay (~1 min), see *Materials and Methods*. The resulting kinetic parameters are given in Table 1 and for the substrate isotope effects.

One expects an increase in mass of the substrate to alter the frequency of the C-H stretch in both the ground and transition state, but whether the expected change still manifests in the presence of the active site amino acids is not obvious. Therefore, we have performed frequency calculations on the stationary points obtained from the above cluster model (Figure 1C), for each of the isotopically substituted states shown in Figures 4 and S1. The resulting frequencies are given in Table S1. We find a large decrease in stretching frequencies of both the TS and ground state on deuteration of the transferred hydride. On additional isotopic substitution there is generally a small decrease in the C-H stretching frequency for both the ground state and the TS. Again, one expects small changes in frequency on increasing mass through isotopic substitution and our calculations suggest this expected trend is preserved when the first shell of protein amino acids is also present (as in Figure 1C). It is interesting to note that where the amino acids are deuterated (solvent exchangeable positions as with our experiments conducted in D_2O), the frequencies show an additional and significant effect on the calculated frequencies in the order of ~1 cm^{-1}. We would stress that clearly elucidating the relationship between the change in frequencies at the ground/TS, the protein and $\Delta\Delta C_P^{\ddagger}$ would require very extensive (QM/MM) simulation studies.

There is a significant effect of increased isotope substitution on both the magnitude of the observed rate but also the magnitude of $\Delta C_P^{\ddagger}$ (Figure 4A and Table 1). From Figure 4B, the KIE increases with increasing isotopic substitution, but not in a linear fashion. The absolute magnitude of the KIE depends on the temperature at which the value is reported, the different contributions from substitutions at different positions and the fact that the temperature dependence of the isotope effects is different for different isotopic substitutions (Table 1). Therefore, one does not necessarily expect the values to follow an obvious e.g. linear trend. That said, the maximal KIE does tend to increase with increased isotopic substitution, except in the case of Gluc-D_7 (Figure 4D) and we note the relatively large error on these values. As with the 1° KIE, we observe curvature in the magnitude of the KIE for all our isotopic labelling patterns. Figure S3 shows the resulting curve from both fits of the data to Eq 1 and Eq 2, and the corresponding extracted data are given in Table 1.

Given the complex nature of the isotopic labelling pattern for each isotopologue, we do not wish to overinterpret the microscopic contributions to the absolute magnitude of the KIEs. However, it is worth noting that comparison of Gluc-D12 with Gluc-D1 should reveal the combined influence of the secondary substitutions, where a 'normal' secondary KIE would be in the region ~1.1. These effects should be additive, i.e. the individual KIEs should be multiplied: 2.1 ± 0.6 × 1.1 × 1.1 ≈ 2.5 ± 0.6 which differs from the result observed (~3.7 ± 1.1). The large value suggests a significant contribution from secondary effects (~1.3 – 1.4). Huskey and Schowen have suggested that large enzyme secondary

KIEs reflect strong 'vibrational coupling' of the secondary sites to the reaction coordinate at the transition state.[35] More recent studies combining density functional theory (DFT) calculations of a model enzyme secondary KIE with high pressure measurements have similar findings.[36] We note that the notion of vibrational coupling is itself problematic and we do not suggest that our data reflect such coupling, not least because no study has provided unequivocal evidence for so called vibrational coupling. Given our data we cannot confidently assign the origin of these apparently exalted secondary KIEs.

The calculated KIEs from our QM cluster model (Table 1), suggest an expected secondary KIE of ~3.4 ($2.8 \times 1.1 \times 1.1$), which differs from the calculated value of 2.3 (Table 1). That is, the secondary KIE value is not as expected for either the experimental measurements or QM calculations. Given the excellent agreement between the experimentally measured and calculated 1° KIE (Table 1), the data may indicate that the limitations of the (static) QM cluster model and the importance of enzyme KIEs being calculated using as full a structural model, including conformational sampling, as possible. However, we note that the differences in the absolute magnitude of the experimental KIEs are in fact relatively small, particularly when taking into account the experimental error as shown in Figure 4B. As we state above, given this limitation, we prefer a more conservative interpretation of the labelling study, focusing on the increase in isotopic mass rather than the absolute contributions to the KIE from each labelled atom. Figure 4C shows the relationship between the extracted $\Delta C_P^{\ddagger}$ values (from Figure 4A) and the increase in isotopic mass of the substrate. From Figure 4C, the isotope effect on $\Delta C_P^{\ddagger}$ appears to increase with respect to the mass of the glucose. These data appear to show saturation behavior, with $\Delta C_P^{\ddagger}$ trending towards zero with increasing isotopic mass. Whilst the initial change in $\Delta C_P^{\ddagger}$ is relatively large for just one mass unit increase (Gluc-D_1. $\Delta\Delta C_P^{\ddagger}$ = 2.2 ± 1 kJ mol^{-1} K^{-1}), we find large (~1 kJ mol^{-1} K^{-1}) changes in $\Delta C_P^{\ddagger}$ associated with further isotopic substitutions.

Frequency calculations from the QM cluster model indicate these additional increases in mass (D_5-D_{12}) should only change the frequencies of the reacting species (and immediate surrounding) at the ground and transition state by at most a few wavenumbers (Table S1). Moreover, the calculated $\Delta C_P^{\ddagger}$ values are 3 orders of magnitude smaller than measured experimentally (Table S2). Finally, the calculated KIEs from the QM cluster model show essentially no curvature (Figure S4) compared to the clear curvature observed experimentally (Figure 4B) and shown by comparative fitting of Eq 1 and Eq 2 in Figure S3. A simplistic conclusion from these data would be that our experimental data are not reflecting vibrational frequency changes on isotopic substitution. However, the difference between experimental and computational values is that the QM cluster model neglects nearly all the protein. Recent molecular dynamics simulations that correctly predict significant enzyme $\Delta C_P^{\ddagger}$ values (~kJ mol^{-1} K^{-1}) have shown that the $\Delta C_P^{\ddagger}$ arises from energetic fluctuations across the whole molecule, including domains distant from the active site.[18] It therefore seems likely that the large isotope effect on $\Delta C_P^{\ddagger}$ has a major component arising from changes in protein fluctuations further removed from the active site.

CONCLUSIONS

We have monitored the isotope effect on $\Delta C_P^{\ddagger}$ for a hypethermophilic enzyme, finding a very large primary isotope effect on the magnitude of $\Delta C_P^{\ddagger}$ for two different substrates (glucose and xylose). The size of the isotope effect on $\Delta C_P^{\ddagger}$ is very much larger than predicted based on a QM cluster model. Further we illustrate an additive effect of increase the isotopic mass of glucose on the magnitude of $\Delta C_P^{\ddagger}$. Taken together, our data shows that the change in $\Delta C_P^{\ddagger}$ is coincident with an increase in isotopic mass. These significant changes in $\Delta C_P^{\ddagger}$ (~ 1-2 kJ mol^{-1} K^{-1}) are accompanied by only small (~1 cm^{-1}) changes in vibrational frequency of the reacting species. If the change in $\Delta C_P^{\ddagger}$ arises from these small-scale frequency changes there would need to be some significant 'amplification' of the small local effect. Therefore, the key question arising from the mass modulation data presented here is what is behind the isotopic mass dependence on $\Delta C_P^{\ddagger}$ (Figure 4C). Specifically, if a significant change in enzymatic $\Delta C_P^{\ddagger}$ (and $\Delta H^{\ddagger}$; Table 1), on the ~kJ mol^{-1} K^{-1} scale arises when there are only small changes (on the ~1 cm^{-1} scale) in the vibrational frequency of the ground and transition states of the reacting species, how might this occur?

A similar conceptual challenge arises from protein mass modulation studies where changing the mass of a protein by isotopic substitution (mass change of ~10%) gives rise to very large changes in the temperature dependence of the rate (isotope effect on $\Delta H^{\ddagger}$, $\Delta\Delta H^{\ddagger}$, changes by ~0-10 kJ mol^{-1}). These very large changes are difficult to rationalize since the expected change in the frequency of protein vibrational modes (for a protein that is ~10 % increase in mass) is on the scale of only a few wavenumbers. Previous efforts to interpret such data have suggested that large changes in $\Delta H^{\ddagger}$ might be achieved where protein vibrational modes become 'decoupled' from the enzyme catalyzed chemistry.[28,37,38] Ranasinghe *et al* have recently extended this rationale by suggesting that mass modulation not only affects protein motions coupled to the enzyme catalyzed chemical step, but also the electrostatics associated with longer timescale events during turnover.[39] We note that these works have not considered $\Delta C_P^{\ddagger}$. Moreover, there have been a significant number of studies that suggest that protein 'dynamics' do not affect enzyme catalysis[17,40–43] and are not in any way coupled to the reaction coordinate.

Our study provides a fresh perspective on current hypotheses that seek to understand the relationship between enzyme vibrational modes and (the temperature dependence of) catalysis, incorporating a difference in enzyme heat capacity (and thus vibrational modes) along the reaction, $\Delta C_P^{\ddagger}$.

Our data point to a model that links small changes in the vibrational modes of the substrate (or reacting species) to large changes in enzyme fluctuations in different states along the reaction. $\Delta C_P^{\ddagger}$ reflects the change in the *distribution* (and/or magnitude) of protein vibrational modes between the ground and transition state. Therefore, we expect that the apparent disconnect between the scale of substrate isotopic mass changes and the (thermodynamic) heat capacity changes might be resolved by a deeper understanding of the distribution of these protein vibrational modes and how these modes are affected by subtle changes in substrate vibrations. For example, based on our present understanding of the physical origin of $\Delta C_P^{\ddagger}$, we suggest a physical model where the isotopic changes in the substrate are translated to a shift in the conformational landscape (structural, energetic or both) of the enzyme, resulting in a difference in fluctuations between the reactant and transition state complexes.[15]

MATERIALS AND METHODS

ssGDH expression and purification. *ss*GDH was expressed with AmpR in a pET3a plasmid. It was transformed into BL21 (DE3) *Escherichia coli* using heat shock and grown on LB agar with ampicillin (100 μg/ml) at 37 °C. A 50 ml LB starter culture was used to inoculate 5 x 1L LB until an OD_{600} of 0.5-0.6 was reached. Cells were harvested by centrifugation (4 °C, 8000 rpm, 10 min) before being lysed by sonication using a lysis buffer (pH 7) containing 100 mM HEPES, lysozyme, DNAase and a protease inhibitor cocktail tablet. Soluble and insoluble fractions were separated by centrifugation at 4 °C (25,000 rpm, 10 min). Due to the thermostability of *ss*GDH, the soluble fraction was purified by heating the sample to 70 °C for 50 min. To remove precipitated protein, samples were centrifuged (4 °C 13,000 rpm, 10 min) before being dialysed for 4 hours in 100 mM HEPES buffer (pH 7). Samples were further purified/concentrated through the use of Vivaspin centrifugal concentrators (MWCO = 30 kDa). The concentration of purified samples was measured by the absorbance at 280 nm (ε280 = 49,390 M^{-1} cm^{-1}), obtained via the input of *ss*GDH amino acid sequence into the ExPASy ProtParam tool.[44] Approximately 8 ml of 35 mg/ml purified sample was obtained.

Substrates and coenzymes. D-glucose, D-xylose, D_2O and $NADP^+$ were obtained from Sigma Aldrich. D-glucose (1-D), D-glucose (1,2,3,4,5,6,6-D7) and D-xylose (1-D) were obtained from Cambridge Isotope Laboratories. In this manuscript the varying isotopes and D_2O combinations will be described with the following nomenclature: D-glucose (1-D) – D_1 , D-xylose (1-D) – D_1, D-glucose + D_2O – D_5 , D-glucose (1,2,3,4,5,6,6-D7) – D_7 , D-glucose (1,2,3,4,5,6,6-D7) + D_2O – D_{12}.

Enzyme assays. Steady-state *ss*GDH kinetic measurements were carried out using a lidded 1 ml quartz cuvette to prevent evaporation at high temperatures and a UV/ Vis spectro-photometer (Agilent Cary 60 UV-Vis spectrometer) in 100 mM HEPES (pH 8). Accurate concentrations of $NADP^+$ were determined using NADP ε_{260} = 17,800 M^{-1} cm^{-1}. Enzyme activity was measured for each condition at 85 °C by following the formation of NADPH at 340 nm using ε_{340} = 6220 M^{-1} cm^{-1} as a direct measurement of ssGDH steady-state rates ; the data fitted well to Michaelis-Menten kinetics. Temperature dependences were carried out from 60 °C – 90 °C at 5 °C intervals using initial velocity measurements at substrate concentrations maintained above 10x K_m to ensure saturation. The data were fitted to Eq 1 or Eq 2 as described in the manuscript using OriginPro 2016 (MicroCal). The measured pH for experiments performed in D_2O was adjusted accordingly to match that of the pH in H_2O.[45]

Molecular dynamics simulations. The *ss*GDH crystal structure 2CDB[30] was prepared for simulation using scwrl4[46] to revert the T41A mutation and modeller[47] to model in the missing loop at positions 50-59 (based on chain A). To obtain similar starting points for the glucose and xylose complexes, this loop was used for all four chains and coordinates from 2CDB were also used for the xylose complex (where xylose was placed based on alignment with 2CDC[30]). The Amber16 suite of programs was used for periodic boundary simulation and analysis[48], with the ff14SB force-field for protein atoms[49], GLYCAM-06j for glucose/xylose[50], parameters from Ryde *et al.* for NADP+,[51] TIP3P for water and ZAFF[52] for the Zn^{2+} coordinated by Cys93, Cys96, Cys99 and Cys107. For the Zn^{2+} directly adjacent to the substrate binding site, restraints were used to maintain the crystallographically observed coordination with Cys39 and His66. After brief minimization of the complex and added water, the system was heated to 300 K and subsequently equilibrated to 1 atm in the NPT ensemble (with positional restraints on Cα atoms). After gradual release of Cα positional restraints, 50 ns NPT production simulations were performed at 300 K and 1 atm. Histograms of the D-A distances were calculated over all four binding sites using 10-50 ns of four independent simulations for each substrate. (Further details of model setup, restraints and simulation procedures are included in the Supporting Information.)

QM Cluster Model. The aforementioned X-ray crystal structure of *ss*GDH in complex with glucose and $NADP^+$ (PDB ID 2CDB[30]) was used to create a 148 atom model of the active site (Figure S5). To preserve the overall structure of the active site, several atoms were fixed throughout the optimisation process and care was taken to ensure non-reacting groups stayed in the same local minima throughout the reaction. The T41A mutation was reversed *in silico* with the rotamer selected based on our MD simulations. All Calculations were performed using Gaussian16,[53] employing the M06-2X functional.[54] Geometry optimisations and frequency calculations were performed *in vacuo* with the 6-

31G(d,p) basis set. All models were optimised on an ultrafine integration grid and under tight convergence criteria. Single point energies were obtained using the 6-311++G(2d,2p) basis set, with the surrounding protein environment accounted for using the SMD solvation model with a dielectric constant of 4.[55] Thermal corrections to the obtained energies were taken from the aforementioned frequency calculations, employing a scale factor of 0.97.[56] Contributions to tunneling on the rate of reaction were estimated using Wigner's correction.[57] Further details about calculation methodology and the coordinates of all stationary points obtained can be found in the Supporting Information.

ASSOCIATED CONTENT

Supporting Information. Molecular dynamics simulations, QM cluster model calculations, supporting data and cartesian coordinates of all stationary points. This material is available free of charge via the Internet at http://pubs.acs.org.

AUTHOR INFORMATION

Corresponding Author

*Christopher R Pudney, Department of Biology and Biochemistry, University of Bath, Bath, United Kingdom. c.r.pudney@bath.ac.uk.
*Marc W van der Kamp, School of Biochemistry, University of Bristol, Cantock's Close, Bristol BS8 1TS, United Kingdom. marc.vanderkamp@bristol.ac.uk.
*Vickery L Arcus, School of Science, Faculty of Science and Engineering, University of Waikato, Hamilton 3240, New Zealand. varcus@waikato.ac.nz.

Author Contributions

HBLJ and CM performed experimental work. RMC, MWK and ABT performed computational simulations and calculations. All authors discussed and interpreted data. The manuscript was written through contributions of all authors. All authors have given approval to the final version of the manuscript. Δ, these authors contributed equally.

ABBREVIATIONS

D-glucose (1-D), D_1 ; D-xylose (1-D), D_1 ; D-glucose + D_2O, D_5 ; D-glucose (1,2,3,4,5,6,6-D7) , D_7 ; D-glucose (1,2,3,4,5,6,6-D7) + D_2O, D_{12}.

ACKNOWLEDGMENT

HBLJ's studentship is funded by the University of Bath. RMC's studentship is funded by the EPSRC. MWvdK is a BBSRC David Phillips Fellow (BB/M026280/1). We thank Katarzyna Świderek (Universitat Jaume I), Ian H. Williams (University of Bath) and Vicent Moliner (Universitat Jaume I) for helpful discussions and critical review of the manuscript.

REFERENCES

(1) Cook, P. F. Mechanism from Isotope Effects. *Isot. Environ. Health Stud.* **1998**, *34*, 3–17.
(2) Schwartz, S. D.; Schramm, V. L. Enzymatic Transition States and Dynamic Motion in Barrier Crossing. *Nat. Chem. Biol.* **2009**, *5*, 551–558.
(3) Allemann, R. K.; Evans, R. M.; Tey, L.; Maglia, G.; Pang, J.; Rodriguez, R.; Shrimpton, P. J.; Swanwick, R. S. Protein Motions during Catalysis by Dihydrofolate Reductases. *Philos. Trans. R. Soc., B* **2006**, *361*, 1317–1321.
(4) Luk, L. Y. P.; Javier Ruiz-Pernia, J.; Dawson, W. M.; Roca, M.; Loveridge, E. J.; Glowacki, D. R.; Harvey, J. N.; Mulholland, A. J.; Tunon, I.; Moliner, V.; Allemann, R. K. Unraveling the Role of Protein Dynamics in Dihydrofolate Reductase Catalysis. *Proc. Natl. Acad. Sci. U. S. A.* **2013**, *110*, 16344–16349.
(5) Thornton, E. R. Physical Organic Chemistry. *Annu. Rev. Phys. Chem.* **1966**, *17*, 349–372.
(6) Knapp, M. J.; Klinman, J. P. Environmentally Coupled Hydrogen Tunneling. *Eur. J. Biochem.* **2002**, *269*, 3113–3121.
(7) Knapp, M. J.; Rickert, K.; Klinman, J. P. Temperature-Dependent Isotope Effects in Soybean Lipoxygenase-1: Correlating Hydrogen Tunneling with Protein Dynamics. *J. Am. Chem. Soc.* **2002**, *124*, 3865–3874.
(8) Roy, S.; Schopf, P.; Warshel, A. Origin of the Non-Arrhenius Behavior of the Rates of Enzymatic Reactions. *J. Phys. Chem. B* **2017**, *121*, 6520–6526.
(9) Francis, K.; Sapienza, P. J.; Lee, A. L.; Kohen, A. The Effect of Protein Mass Modulation on Human Dihydrofolate Reductase. *Biochemistry* **2016**, *55*, 1100–1106.
(10) Wang, Z.; Singh, P.; Czekster, C. M.; Kohen, A.; Schramm, V. L. Protein Mass-Modulated Effects in the Catalytic Mechanism of Dihydrofolate Reductase: Beyond Promoting Vibrations. *J. Am. Chem. Soc.* **2014**, *136*, 8333–8341.
(11) Kipp, D. R.; Silva, R. G.; Schramm, V. L. Mass-Dependent Bond Vibrational Dynamics Influence Catalysis by HIV-1 Protease. *J. Am. Chem. Soc.* **2011**, *133*, 19358–19361.
(12) Soriano, A.; Silla, E.; Tuñón, I.; Martí, S.; Moliner, V.; Bertrán, J. Electrostatic Effects in Enzyme Catalysis: A Quantum Mechanics/molecular Mechanics Study of the Nucleophilic Substitution Reaction in Haloalkane Dehalogenase. *Theor. Chem. Acc.* **2004**, *112*, 327–334.
(13) García-Meseguer, R.; Martí, S.; Ruiz-Pernía, J. J.; Moliner, V.; Tuñón, I. Studying the Role of Protein Dynamics in an SN2 Enzyme Reaction Using Free-Energy Surfaces and Solvent Coordinates. *Nat. Chem.* **2013**, *5*, 566–571.
(14) Olsson, M. H. M.; Parson, W. W.; Warshel, A. Dynamical Contributions to Enzyme Catalysis: Critical Tests of A Popular Hypothesis. *Chem. Rev.* **2006**, *106*, 1737–1756.
(15) Åqvist, J.; Kazemi, M.; Isaksen, G. V.; Brandsdal, B. O. Entropy and Enzyme Catalysis. *Acc. Chem. Res.* **2017**, *50*, 199–207.
(16) Schramm, V. L.; Schwartz, S. D. Promoting Vibrations and the Function of Enzymes. Emerging Theoretical and Experimental Convergence. *Biochemistry* **2018**, *In press*.
(17) Warshel, A.; Bora, R. P. Perspective: Defining and Quantifying the Role of Dynamics in Enzyme Catalysis. *J. Chem. Phys.* **2016**, *144*, 180901.
(18) van der Kamp, M. W.; Prentice, E. J.; Kraakman, K. L.; Connolly, M.; Mulholland, A. J.; Arcus, V. L. Dynamical Origins of Heat Capacity Changes in Enzyme-Catalysed Reactions. *Nat. Commun.* **2018**, *9*, 1177.
(19) Jones, H. B. L.; Wells, S. A.; Prentice, E. J.; Kwok, A.; Liang, L. L.; Arcus, V. L.; Pudney, C. R. A Complete Thermodynamic Analysis of Enzyme Turnover Links the Free Energy Landscape to Enzyme Catalysis. *FEBS J.* **2017**, *284*, 2829–2842.
(20) Arcus, V. L.; Pudney, C. R. Change in Heat Capacity Accurately Predicts Vibrational Coupling in Enzyme Catalyzed Reactions. *FEBS Lett.* **2015**, *589*, 2200–2206.
(21) Hobbs, J. K.; Jiao, W.; Easter, A. D.; Parker, E. J.; Schipper, L. a.; Arcus, V. L. Change in Heat Capacity for Enzyme Catalysis Determines Temperature Dependence of Enzyme Catalyzed Rates. *ACS Chem. Biol.* **2013**, *8*, 2388–2393.
(22) Arcus, V. L.; Prentice, E. J.; Hobbs, J. K.; Mulholland, A. J.; van der Kamp, M. W.; Pudney, C. R.; Parker, E. J.; Schipper, L. A. On the Temperature Dependence of Enzyme-Catalyzed Rates.

Biochemistry **2016**, *55*, 1681–1688.
(23) Daniel, R. M.; Danson, M. J.; Eisenthal, R.; Lee, C. K.; Peterson, M. E. The Effect of Temperature on Enzyme Activity: New Insights and Their Implications. *Extremophiles* **2008**, *12*, 51–59.
(24) Glowacki, D. R.; Harvey, J. N.; Mulholland, A. J. Taking Ockham's Razor to Enzyme Dynamics and Catalysis. *Nat. Chem.* **2012**, *4*, 169–176.
(25) Bigeleisen, J. Effect of Isotopic Substitution on the Entropy, Enthalpy, and Heat Capacity of Ideal Gases. I. Systems in Thermal Equilibrium. II. Chemically Reacting Systems. *J. Chem. Phys.* **1953**, *21*, 1333–1339.
(26) Tjahjono, M.; Garland, M. Deuterium Isotope Effect on Molar Heat Capacities and Apparent Molar Heat Capacities in Dilute Aqueous Solutions: A Multi-Channel Heat-Flow Microcalorimeter Study. *J. Chem. Thermodyn.* **2008**, *40*, 1600–1606.
(27) Ibberson, R. M.; David, W. I. F.; Yamamuro, 0; Miyoshi, Y.; Matsuo, T.; Suga, H. Calorimetric, Dielectric, and Neutron Diffraction Studies on Phase Transitions in Ordinary and Deuterated Acetone Crystals'. *J. Phys. Chem* **1995**, *99*, 14167–14173.
(28) Longbotham, J. E.; Hardman, S. J. O.; Görlich, S.; Scrutton, N. S.; Hay, S. Untangling Heavy Protein and Cofactor Isotope Effects on Enzyme-Catalyzed Hydride Transfer. *J. Am. Chem. Soc.* **2016**, *138*, 13693–13699.
(29) Lamble, H.; Heyer, N.; Bull, S.; Hough, D. Metabolic Pathway Promiscuity in the Archaeon Sulfolobus Solfataricus Revealed by Studies on Glucose Dehydrogenase and 2-Keto-3-Deoxygluconate Aldolase. *J. Biol.* **2003**, *278*, 34066–34072.
(30) Milburn, C. C.; Lamble, H. J.; Theodossis, A.; Bull, S. D.; Hough, D. W.; Danson, M. J.; Taylor, G. L. The Structural Basis of Substrate Promiscuity in Glucose Dehydrogenase from the Hyperthermophilic Archaeon Sulfolobus Solfataricus. *J. Biol. Chem.* **2006**, *281*, 14796–14804.
(31) Blomberg, M. R. A.; Borowski, T.; Himo, F.; Liao, R.-Z.; Siegbahn, P. E. M. Quantum Chemical Studies of Mechanisms for Metalloenzymes. *Chem. Rev.* **2014**, *114*, 3601–3658.
(32) Giardina, P.; De Biasi, M.-G.; De Rosa, M.; Gambacortat, A.; Buonocore, V. Glucose Dehydrogenase from the Thermoacidophilic Archaebacterium Sulfolobus Solfataricus. *Biochem. J* **1986**, *239*, 517–522.
(33) Pudney, C.; Johannissen, L.; Sutcliffe, M. Direct Analysis of Donor– Acceptor Distance and Relationship to Isotope Effects and the Force Constant for Barrier Compression in Enzymatic H-Tunneling Reactions. *J. Am. Chem. Soc.* **2010**, *132*, 11329–11335.
(34) Moser, C. C.; Dutton, P. L. Engineering Protein Structure for Electron Transfer Function in Photosynthetic Reaction Centers. *Biochim. Biophys. Acta, Bioenerg.* **1992**, *1*, 171–176.
(35) Huskey, W. P.; Schowen, R. L. Reaction-Coordinate Tunneling in Hydride-Transfer Reactions. *J. Am. Chem. Soc.* **1983**, *105*, 5704–5706.
(36) Hay, S.; Pudney, C. R.; Sutcliffe, M. J.; Scrutton, N. S. Probing Active Site Geometry Using High Pressure and Secondary Isotope Effects in an Enzyme-Catalysed "deep" H-Tunnelling Reaction. *J. Phys. Org. Chem.* **2010**, *23*, 696–701.
(37) Pudney, C. R.; Guerriero, A.; Baxter, N. J.; Johannissen, L. O.; Waltho, J. P.; Hay, S.; Scrutton, N. S. Fast Protein Motions Are Coupled to Enzyme H-Transfer Reactions. *J. Am. Chem. Soc.* **2013**, *135*, 2512–2517.
(38) Antoniou, D.; Ge, X.; Schramm, V. L.; Schwartz, S. D. Mass Modulation of Protein Dynamics Associated with Barrier Crossing in Purine Nucleoside Phosphorylase. *J. Phys. Chem. Lett.* **2012**, *3*, 3538–3544.
(39) Ranasinghe, C.; Guo, Q.; Sapienza, P. J.; Lee, A. L.; Quinn, D. M.; Cheatum, C. M.; Kohen, A. Protein Mass Effects on Formate Dehydrogenase. *J. Am. Chem. Soc.* **2017**, *139*, 17405–17413.
(40) Jordi, V.; Warshel, A. Energetics and Dynamics of Enzymatic Reactions. *J. Phys. Chem. B* **2001**, *105*, 7887–7907.
(41) Pisliakov, A. V.; Cao, J.; Kamerlin, S. C. L.; Warshel, A. Enzyme Millisecond Conformational Dynamics Do Not Catalyze the Chemical Step. *Proc. Natl. Acad. Sci. U. S. A.* **2009**, *106*, 17359–17364.
(42) Boekelheide, N.; Salomón-Ferrer, R.; Miller, T. F. Dynamics and Dissipation in Enzyme Catalysis. *Proc. Natl. Acad. Sci. U. S. A.* **2011**, *108*, 16159–16163.
(43) Loveridge, E. J.; Behiry, E. M.; Guo, J.; Allemann, R. K. Evidence That a "dynamic Knockout" in Escherichia Coli Dihydrofolate Reductase Does Not Affect the Chemical Step of Catalysis. *Nat. Chem.* **2012**, *4*, 292–297.
(44) Gasteiger, E.; Hoogland, C.; Gattiker, A.; Duvaud, S.; Wilkins, M. R.; Appel, R. D.; Bairoch, A. *Protein Identification and Analysis Tools on the ExPASy Server*; Humana press: USA, 2005.
(45) Mikkelsen, K.; Siguri, A.; Nielsen, O. Acidity Measurements Jyith the Glass Electrode Is H,o-D,o Mixtures. *J. Phys. Chem.* **1960**, *64*, 632–637.
(46) Krivov, G. G.; Shapovalov, M. V.; Dunbrack, R. L. Improved Prediction of Protein Side-Chain Conformations with SCWRL4. *Proteins: Struct., Funct., Bioinf.* **2009**, *77*, 778–795.
(47) Webb, B.; Sali, A.; Webb, B.; Sali, A. Comparative Protein Structure Modeling Using MODELLER. In *Protein Structure Prediction*; John Wiley & Sons, Inc.: Hoboken, NJ, USA, 2014; pp 1–15.
(48) Case, D. A.; Cerutti, D. S.; Cheatham, III, T. E.; Darden, T. A.; Duke, R. E.; Giese, T. J.; Gohlke, H.; Goetz, A. W.; Greene, D.; Homeyer, N,; Izadi, S.; Kovalenko, A.; Lee, T. S.; LeGrand, S.; Li, P.; Lin, C.; Liu, J.; Luchko, T.; Luo, R.; Mermelstein, D.; Merz, K. M.; Monard, G.; Nguyen, H.; Omelyan, I.; Onufriev, A.; Pan, F.; Qi, R.; Roe, D. R.; Roitberg, A.;Sagui, C.; Schott-Verdugo, S.; Shen, J.; Simmerling, C. L.; Smith, J.; Swails, J.; Walker, R. C.; Wang, J.; Wei, H.; Wolf, R. M.; Wu, X.; Xiao, L.; York D. M.; Kollman, P. A. AMBER 2016. University of Calafornia: San Francisco 2017.
(49) Maier, J. A.; Martinez, C.; Kasavajhala, K.; Wickstrom, L.; Hauser, K. E.; Simmerling, C. ff14SB: Improving the Accuracy of Protein Side Chain and Backbone Parameters from ff99SB. *J. Chem. Theory Comput.* **2015**, *11*, 3696–3713.
(50) Kirschner, K. N.; Yongye, A. B.; Tschampel, S. M.; González-Outeiriño, J.; Daniels, C. R.; Foley, B. L.; Woods, R. J. GLYCAM06: A Generalizable Biomolecular Force Field. Carbohydrates. *J. Comput. Chem.* **2008**, *29*, 622–655.
(51) Holmberg, N.; Ryde, U.; Bülow, L. Redesign of the Coenzyme Specificity in L-Lactate Dehydrogenase from Bacillus Stearothermophilus Using Site-Directed Mutagenesis and Media Engineering. *Protein Eng.* **1999**, *12*, 851–856.
(52) Peters, M. B.; Yang, Y.; Wang, B.; Füsti-Molnár, L.; Weaver, M. N.; Merz, K. M. Structural Survey of Zinc-Containing Proteins and Development of the Zinc AMBER Force Field (ZAFF). *J. Chem. Theory Comput.* **2010**, *6*, 2935–2947.
(53) Frisch, M. J.; Trucks, G. W.; Schlegel, H. B.; Scuseria, G. E.; Robb, M. A.; Cheeseman, J. R.; Scalmani, G.; Barone, V.; Petersson, G. A.; Nakatsuji, H.; Li, X.; Caricato, M.; Marenich, A. V.; Bloino, J.; Janesko, B. G.; Gomperts, R.; Mennucci, B.; Hratchian, H. P.; Ortiz, J. V.; Izmaylov, A. F.; Sonnenberg, J. L.; Williams-Young, D.; Ding, F.; Lipparini, F.; Egidi, F.; Goings, J.; Peng, B.; Petrone, A.; Henderson, T.; Ranasinghe, D.; Zakrzewski, V. G.; Gao, J.; Rega, N.; Zheng, G.; Liang, W.; Hada, M.; Ehara, M.; Toyota, K.; Fukuda, R.; Hasegawa, J.; Ishida, M.; Nakajima, T.; Honda, Y.; Kitao, O.; Nakai, H.; Vreven, T.; Throssell, K.; Montgomery Jr., J. A.; Peralta, J. E.; Ogliaro, F.; Bearpark, M. J.; Heyd, J. J.; Brothers, E. N.; Kudin, K. N.; Staroverov, V. N.; Keith, T. A.; Kobayashi, R.; Normand, J.; Raghavachari, K.; Rendell, A. P.; Burant, J. C.; Iyengar, S. S.; Tomasi, J.; Cossi, M.; Millam, J. M.; Klene, M.; Adamo, C.; Cammi, R.; Ochterski, J. W.; Martin, R. L.; Morokuma, K.; Farkas, O.; Foresman, J. B.; Fox, D. J. Gaussian 16 Revision 16.A.03. 2016.
(54) Zhao, Y.; Truhlar, D. G. The M06 Suite of Density Functionals for Main Group Thermochemistry, Thermochemical Kinetics, Noncovalent Interactions, Excited States, and Transition Elements: Two New Functionals and Systematic Testing of Four M06-Class Functionals and 12 Other Functionals. *Theor.*

Chem. Acc. **2008**, *120*, 215–241.
(55) Marenich, A. V.; Cramer, C. J.; Truhlar, D. G. Universal Solvation Model Based on Solute Electron Density and on a Continuum Model of the Solvent Defined by the Bulk Dielectric Constant and Atomic Surface Tensions. *J. Phys. Chem. B* **2009**, *113*, 6378–6396.
(56) Alecu, I. M.; Zheng, J.; Zhao, Y.; Truhlar, D. G. Computational Thermochemistry: Scale Factor Databases and Scale Factors for Vibrational Frequencies Obtained from Electronic Model Chemistries. *J. Chem. Theory Comput.* **2010**, *6*, 2872–2887.
(57) Wigner, E. Crossing of Potential Thresholds in Chemical Reactions. *Z. Phys. Chem.* **1932**, *B19*, 203–216.

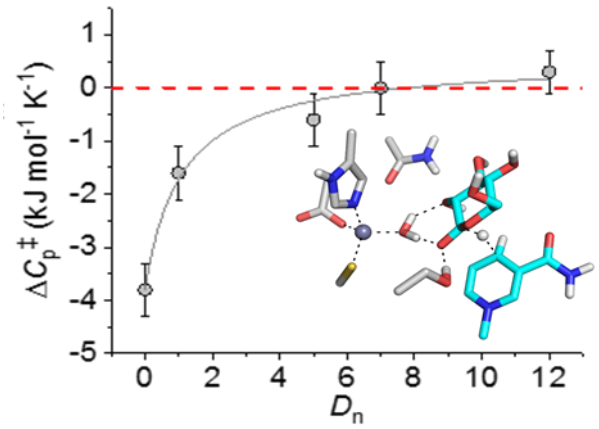
1
0
-1
-2
-3
-4
-5
0
2
4
6
8
10
12
$\Delta C_p^{\ddagger}$ (kJ mol^{-1} K^{-1})
D_n